

## AN ELLIPSOMETRIC STUDY OF THE EFFECTS OF THICKNESS AND SUBSTRATE ON CoCr FILMS

Z.-M. LI AND R. R. PARSONS

*Department of Physics, University of British Columbia, Vancouver, British Columbia V6T 2A6 (Canada)*

(Received August 5, 1988; accepted October 23, 1988)

The effects of thickness and substrate of d.c. magnetron sputtered CoCr films are investigated by spectroellipsometry. The ellipsometric data indicate that the morphology of CoCr films varies as a function of the film thickness and proper choice of substrate can reduce the thickness dependence. It is shown that an NiCr underlayer is capable of reducing the thickness dependence because of its similarity in microstructure to CoCr.

---

### 1. INTRODUCTION

There have been continuing efforts in the research on CoCr thin films for the last ten years owing to their application in both perpendicular and longitudinal recording technologies<sup>1,2</sup>. Recently most attention has been concentrated on CoCr thin films produced by d.c. magnetron sputtering for its convenience in manufacturing<sup>2–12</sup>. It is well known that an initial layer with poor texture is developed for CoCr deposited on glass<sup>3,13</sup>. Previous studies<sup>3,14</sup> show that the magnetic coercivity  $H_{c\perp}$  normal to the film surface depends on both the thickness and the type of substrates. For perpendicular recording application, the initial layer is undesirable and, therefore, it is important to eliminate or reduce the initial layer. In this paper we report a detailed study of the effects of substrate and thickness on CoCr films using ellipsometry for microstructure analysis. Scanning electron microscopy (SEM) and transmission electron microscopy (TEM) are also used to complement the ellipsometry measurements.

The spectroellipsometer used in this study was a rotating-analyzer ellipsometer<sup>15–17</sup> which measured the complex reflection ratio  $\rho = r_p/r_s$ , where  $r_p$  and  $r_s$  are the complex Fresnel reflectance coefficients parallel and perpendicular respectively to the plane of incidence. The dielectric function of the film can be calculated from<sup>15,17</sup>

$$\epsilon = \sin^2\varphi + \sin^2\varphi \tan^2\varphi \left\{ \frac{1-\rho}{1+\rho} \right\}^2 \quad (1)$$

where  $\varphi$  is the angle of incidence. It was found<sup>18–20</sup> that  $\epsilon$  measured in this way is very sensitive to the surface morphology and inhomogeneity of the measured

surface. Comparison of  $\epsilon$  for the thin film measured by ellipsometry with that of the same material in a homogeneous state gives information about the surface morphology or inhomogeneity of the film. Qualitatively, for a rough surface (described by the terminology "microroughness") or a material containing voids full of air or dielectric material (described by "porosity"), the depolarization effect due to the microroughness or porosity reduces the absolute values of  $\epsilon_1$  and  $\epsilon_2$  (real and imaginary parts of  $\epsilon$ ) compared with those of the homogeneous state.

## 2. EXPERIMENTAL DETAILS

A d.c. planar magnetron sputtering system was used to deposit the CoCr thin film samples for this study. An alloyed target 15 cm in diameter with composition of 80 at.% Co and 20 at.% Cr was used. The vacuum system was pumped by a helium cryopump to a base pressure about  $1 \times 10^{-6}$  Torr. The substrate holder assembly held six substrates of size 5 cm  $\times$  5 cm, which were uniformly heated directly behind by a quartz halogen lamp. The substrate temperature  $T_s$  was monitored by a thermocouple attached directly to one of the substrates. By adjusting the heating power, the substrate temperature could be controlled to  $\pm 5$  °C within the range from 25 to 350 °C.

Three types of substrates, glass (Corning 7059), titanium-coated glass, and NiCr (50 at.% Cr) coated glass, were used. NiCr and titanium were sputter deposited on the glass just prior to the CoCr deposition. The thickness of NiCr and titanium films was about 200 nm. The choice of titanium was based on a previous work<sup>21</sup>, which found titanium to be a good substrate material for CoCr. As discussed below, NiCr is shown to be even better than titanium. To improve the film adhesion and reproducibility, the glass substrate was cleaned by a method developed by Sullivan<sup>15</sup>. First, the glass substrates were washed with methanol and rubbed with lens paper. Then the cleaning procedure was repeated with trichloroethylene, followed by methanol again. Finally the substrate was blown dry with an N<sub>2</sub> gas spray.

The sputtering conditions for CoCr thin films were as follows: argon pressure  $P_{Ar} = 3$  mTorr; d.c. sputtering power, 350 W; target-to-substrate distance, 8 cm. After deposition of the films, they were allowed to cool to room temperature and were then quickly removed from the sputtering system and measured on the ellipsometer. Prior to measurement, the films were rinsed with methanol and blown dry with N<sub>2</sub> gas spray. The samples were mounted on a vacuum chuck holder and optically aligned to  $\varphi = 67.50^\circ \pm 0.02^\circ$ . During measurement the polarizer angle was set to  $30.00^\circ \pm 0.02^\circ$ . 80 data points were taken in the spectral range 1.5–6.0 eV. No significant change in the measured dielectric function was observed days or months later when the same sample was re-measured. CoCr and NiCr samples were sputtered onto standard carbon-coated copper grids for TEM studies. SEM was used to examine the surface of the CoCr films.

## 3. RESULTS AND DATA ANALYSIS

Figure 1 gives the coercivity  $H_{c1}$  for the perpendicular magnetization as a

function of CoCr film thickness for the three types of substrate used. The substrate temperature during film growth was  $T_s = 300^\circ\text{C}$ . In the case of glass substrates, the reduced value of  $H_{c\perp}$  for small film thickness has been previously associated<sup>13</sup> with the deposition of an initial layer (about 100 nm) which has poor texture. As seen in Fig. 1, the initial layer effect is not observed in the case of Ti/glass and NiCr/glass substrates. Similar results have been recently obtained by Tanaka and Masuya<sup>21</sup> for CoCr electron beam evaporated on titanium underlayers.

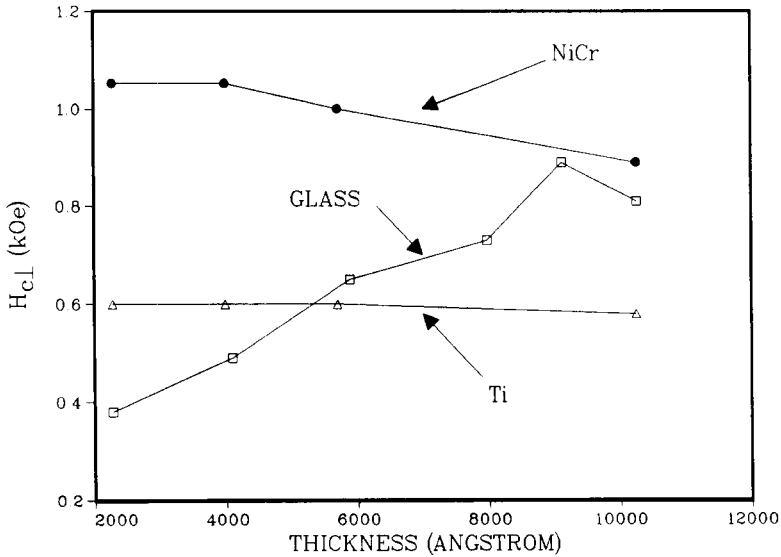


Fig. 1. The substrate effect on the perpendicular magnetic coercivity as a function of film thickness. Sputtering parameters for the samples are  $T_s = 300^\circ\text{C}$ ,  $P_{Ar} = 3\text{ mTorr}$ ,  $W = 350\text{ W}$  and  $d_{cs} = 8\text{ cm}$ . The lines between data points are used only as a guide to the eyes.

Dielectric functions of CoCr films sputtered on unheated glass substrates with deposition conditions described in the last section are shown in Fig. 2 for three different film thicknesses. The decrease in the absolute values of  $\epsilon_1$  and  $\epsilon_2$  indicates increased surface microroughness and/or film porosity with decreasing film thickness. An outline of the effective medium theories used to analyze the data is given below. A more detailed account of the theories can be found elsewhere<sup>18,20</sup>.

Consider a medium that consists of two phases a and b described by dielectric functions  $\epsilon_a$  and  $\epsilon_b$ . The Maxwell-Garnett theory (MGT) gives the effective dielectric function  $\epsilon$  by<sup>18</sup>

$$\frac{\epsilon - \epsilon_b}{\epsilon + 2\epsilon_b} = f_a \frac{\epsilon_a - \epsilon_b}{\epsilon_a + 2\epsilon_b} \tag{2}$$

which is valid only if  $f_a < f_b$ , where  $f_a$  and  $f_b$  are the volume fractions for phases a and b respectively. MGT is most suitable for describing a coated-sphere (cermet) configuration<sup>18</sup>, where inclusions of phase a are completely surrounded by phase b.

The effective-medium approximation (EMA) yields<sup>18</sup>

$$f_a \frac{\epsilon_a - \epsilon}{\epsilon_a + 2\epsilon} + f_b \frac{\epsilon_b - \epsilon}{\epsilon_b + 2\epsilon} = 0, \quad (3)$$

which describes an aggregate model, where particles of phase a and phase b are mixed on a random basis. The theory developed by Sen, Scala and Cohen (SSC)<sup>19,20</sup> incorporates the randomness as well as the coated-particle microstructure and gives

$$\frac{\epsilon - \epsilon_b}{\epsilon_a - \epsilon_b} \left( \frac{\epsilon_a}{\epsilon} \right)^{1/3} = f_a \quad (4)$$

It is common to assume that a sample consists of different layers of material, each of which can be described by a particular effective medium theory. This is the so-called “*N*-layer model”<sup>22</sup>.

There have been reports of chromium and/or cobalt oxides on the surface and the grain boundaries of CoCr<sup>23–25</sup>. However, we are not aware of any dielectric functions of chromium oxides and cobalt oxides. For simplicity we assume that the sputtered CoCr films consist of two phases: homogeneous CoCr with a known value of the dielectric function  $\epsilon_b$  and voids with  $\epsilon_a = 1$ .  $\epsilon_b$  was chosen to be the dielectric function of the sample with the largest value of the dielectric function among the sets of data under consideration, *e.g.* the sample with 870 nm of thickness in Fig. 2. Such a sample was called the “reference sample”. We investigated three different *N*-layer models. (1) The sample is considered to be a single layer of CoCr. This model has only one unknown parameter,  $f_b$ , which is a measure of the sample porosity. (2) The sample consists of a porous top layer with 50% porosity on a layer of CoCr with no porosity. The only unknown parameter in this model is the top layer thickness which is a measure of the microroughness. (3) This is the same as the second model except that the underlying CoCr is now assumed to be porous with an unknown fraction  $f_b$  of CoCr. We further assumed that the same effective medium theory applies to all the layers in an *N*-layer model.

The combination of the above three *N*-layer models with the effective medium theories in eqns. (2)–(4) gives nine possible theoretical models for each set of data. Sullivan<sup>15</sup> has developed elaborate software for the analysis of ellipsometry data which we used to fit the nine models to each set of data. The judgment of a model is based on the following principles. First, it should have a good fit to the data, *i.e.* a small unbiased estimator<sup>17</sup>  $\delta$ . Second, the parameters obtained from the fit should be physically reasonable. Third, given that the goodness of the fit is about the same, the model with smaller number of unknown parameters is chosen so that the interpretation is simpler. The best effective medium theory for the first *N*-layer model was found to be the EMA. Such a fit is shown in Fig. 2. An equally good fit was obtained with the second *N*-layer model but with the use of the SSC theory. Therefore, the same sample can be described either as having a flat surface with porosity or as having a layer with microroughness. The parameters for the fits to the data in Fig. 2 are given in Table I. The third *N*-layer model did not provide a better fit to the data than the first and second models and, therefore, was not pursued.

We also measured the dielectric functions of CoCr sputtered on unheated and heated ( $T_s = 250^\circ\text{C}$ ) NiCr-coated glass as indicated in Figs. 3 and 4. For

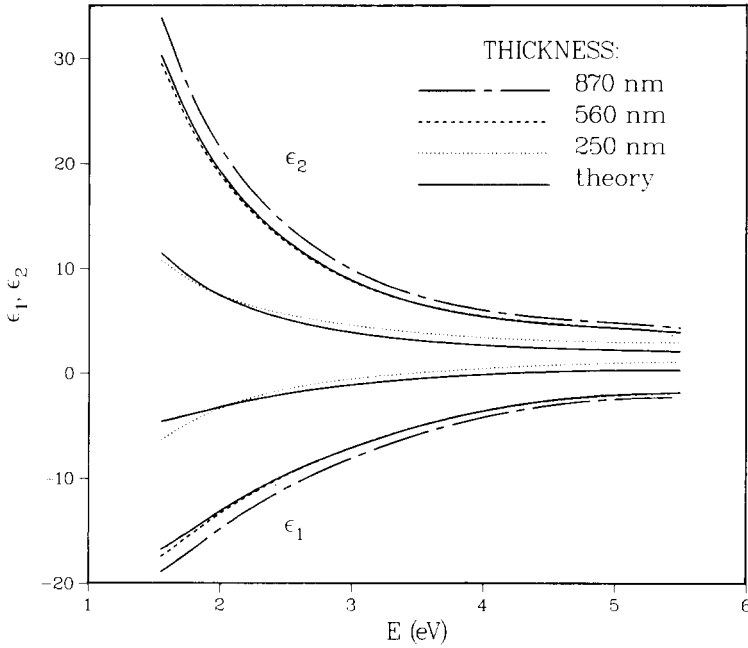


Fig. 2. Real and imaginary parts of the dielectric functions for CoCr sputtered on glass for various film thicknesses. The sputtering parameters are the same as those for Fig. 1 except  $T_s = 30^\circ\text{C}$ : ———, theoretical fit of the EMA assuming a bare substrate. The best-fit values for the volume fraction of CoCr are  $f_b = 55\%$  and  $f_b = 93.1\%$  for samples of thicknesses 250 nm and 560 nm respectively. The reference sample is taken to be the one with 870 nm thickness.

TABLE I  
ANALYSIS OF DATA IN FIG. 2

<i>N</i>	Effective medium theory	CoCr thickness (nm)	$f_b$ (%)	<i>d</i> (nm)	$\delta$
0	EMA	250	$55 \pm 8$		0.080
		560	$93.1 \pm 0.7$		0.003
		870	Reference sample		
1	SSC	250		$19 \pm 10$	0.080
		560		$1.5 \pm 0.2$	0.004
		870	Reference sample		

The films were sputtered on glass. *N* is the number of layers in the *N*-layer model.  $f_b$  is the volume fraction of CoCr. *d* is the top layer thickness in the *N*-layer model, assuming that  $f_b = 50\%$  for the top layer and  $f_b = 100\%$  for the substrate.  $\delta$  is the unbiased estimator for the theoretical fit. 90% confidence limits are also given for the best-fit parameters  $f_b$  and *d*.

comparison the dielectric functions of CoCr deposited on heated (at  $T_s = 250^\circ\text{C}$ ) titanium-coated glass are given in Fig. 5. Using the scheme of data analysis described above, we give the best fit parameters corresponding to Figs. 3, 4 and 5 in Tables II, III and IV respectively. To clarify the relation between dielectric functions and surface morphology, SEM photographs are shown in Figs. 6(a), 6(b) and 6(c)

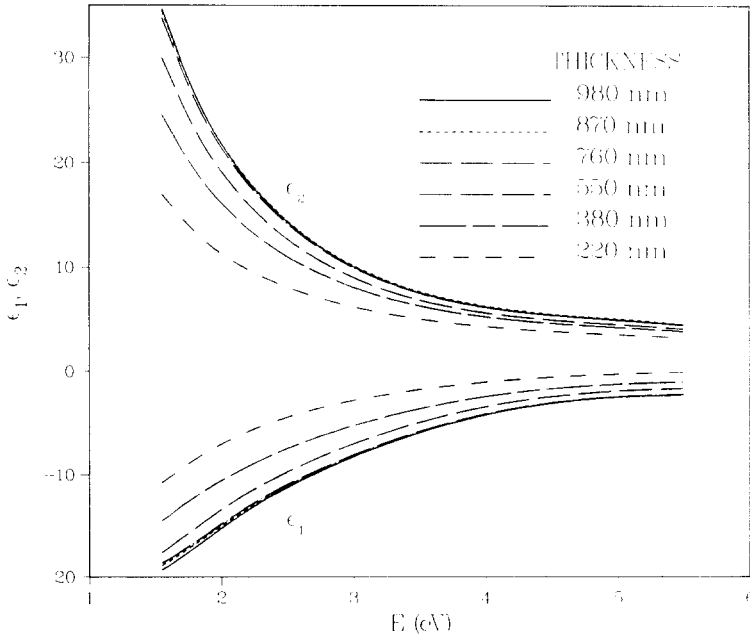


Fig. 3. Dielectric functions for CoCr sputtered on unheated NiCr-coated glass substrate. Deposition parameters are the same as those for Fig. 1 except that  $T_s = 30^\circ\text{C}$ .

TABLE II  
ANALYSIS OF DATA IN FIG. 3

$N$	Effective medium theory	CoCr thickness (nm)	$f_h$ ( $^{\circ}$ )	$d$ (nm)	$\delta$
0	EMA	220	$70 \pm 7$		0.049
		380	$84 \pm 5$		0.028
		550	$92 \pm 2$		0.008
		980	Reference sample		
1	SSC	220		$9.5 \pm 2.9$	0.041
		380		$3.9 \pm 1.2$	0.023
		550		$1.6 \pm 0.3$	0.007
		980	Reference sample		

The films were sputtered on glass. Other details as for Table I.

for respectively CoCr films on unheated NiCr-coated glass with thicknesses of 230 nm, 400 nm and 910 nm. An SEM photograph for CoCr deposited on an NiCr-coated substrate at  $T_s = 250^\circ\text{C}$  is shown in Fig. 6(d). The TEM data in Fig. 7(a) for NiCr deposited on carbon-coated copper grids were used to determine the structure of NiCr underlayers. For comparison the TEM diffraction pattern for CoCr is also shown in Fig. 7(b).

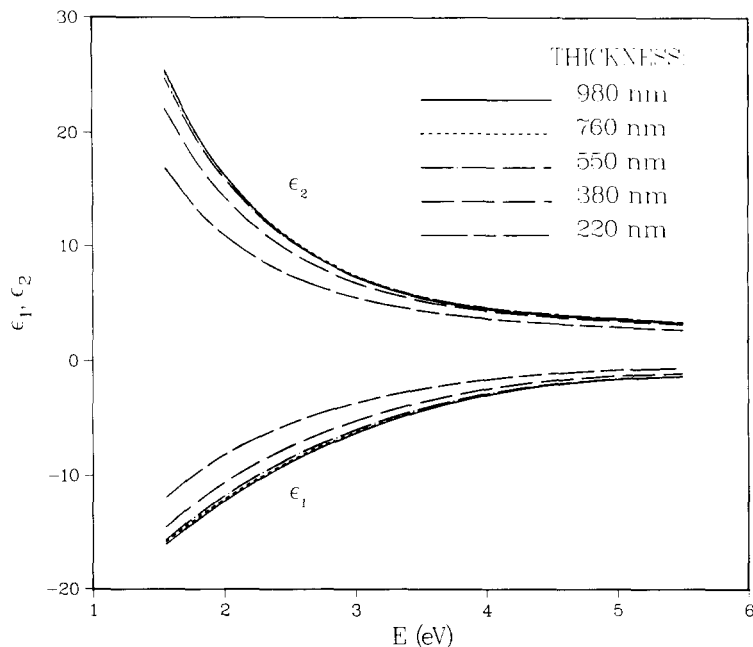


Fig. 4. Dielectric functions for CoCr: details as in Fig. 3 except that  $T_s = 250^\circ\text{C}$ .

TABLE III  
ANALYSIS OF DATA IN FIG. 4

$N$	Effective medium theory	CoCr thickness (nm)	$f_b$ (%)	$d$ (nm)	$\delta$
0	EMA	220	$82 \pm 4$		0.024
		380	$94 \pm 3$		0.014
		980	Reference sample		
1	SSC	220		$5.6 \pm 0.8$	0.012
		380		$1.6 \pm 0.6$	0.010
		980	Reference sample		

Details as for Table II except that substrate temperature is  $250^\circ\text{C}$ .

#### 4. DISCUSSION

The SEM photographs in Figs. 6(a)–6(c) show that films become featureless with increasing thickness. This is consistent with the ellipsometry data which indicated that a rough and/or porous film develops into a smooth and/or dense film with increasing film thickness. As indicated in Figs. 2–5, the dielectric function approached a constant when the film thickness exceeded about 500 nm.

We attribute the decrease in microroughness and/or porosity with increased thickness to the growth of an initial layer with poor texture. Since the preferential growth direction is along the  $c$  axis<sup>26</sup>, grains with randomly distributed  $c$  axes will

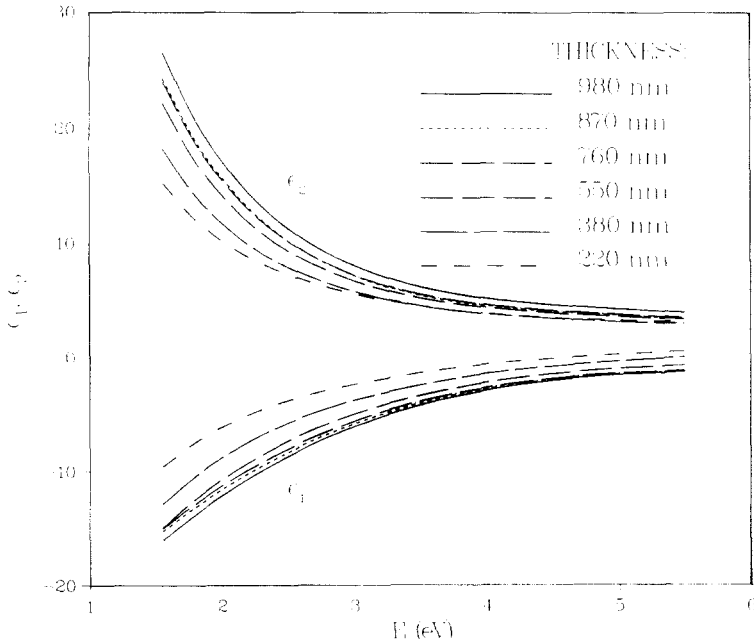


Fig. 5. Dielectric functions for CoCr: details as in Fig. 4 except that the substrate is titanium-coated glass.

TABLE IV  
ANALYSIS OF DATA IN FIG. 5

$N$	Effective medium theory	CoCr thickness (nm)	$f_b$ ( $C_{\infty}$ )	$d$ (nm)	$\delta$
0	EMA	220	$74 \pm 8$		0.052
		380	$80 \pm 3$		0.018
		550	$90 \pm 2$		0.008
		760	$94 \pm 2$		0.010
		870	$94 \pm 3$		0.017
		980	Reference sample		
1	SSC	220		$9 \pm 6$	0.055
		380		$6.1 \pm 1.9$	0.027
		550		$2.7 \pm 0.7$	0.013
		760		$1.4 \pm 0.6$	0.011
		870		$1.3 \pm 0.9$	0.018
		980	Reference sample		

The films were sputtered on titanium-coated glass. Other details as for Table I.

give rise to a porous film structure and/or a rough surface. As the  $c$  axes become better aligned with larger thickness, the grains are more densely packed, resulting in a smoother surface.

The explanation of the results with a heated ( $T_s = 250$  C) substrate follows

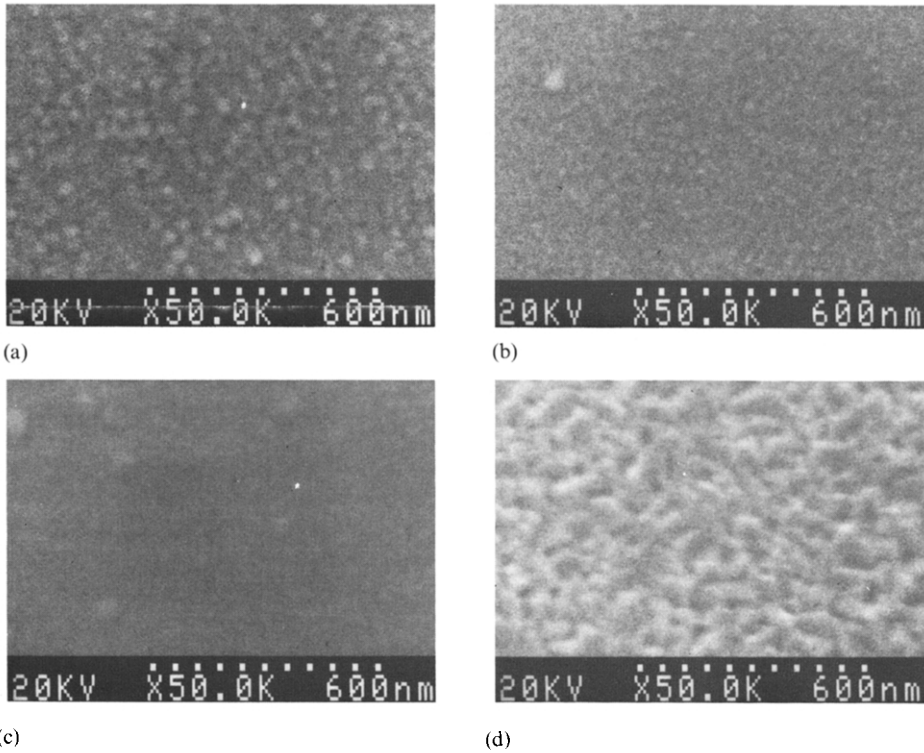


Fig. 6. (a) SEM photograph of the surface of 230 nm thick CoCr sputtered on unheated, NiCr-coated glass substrate. Sputtering conditions are the same as for Fig. 1, except that  $T_s = 30$  C; (b) same as (a) except that the thickness is 400 nm; (c) same as (a) except that the thickness is 910 nm; (d) SEM photograph of surface of 900 nm thick CoCr sputtered on NiCr-coated glass substrate at  $T_s = 250$  C (other sputtering parameters are the same as for Fig. 1). (Magnifications, 50 000  $\times$ .)

closely that of Sullivan who investigated the effects of substrate temperature on the surface morphology of palladium films<sup>15,16</sup>. He interpreted the increase in microroughness and/or porosity in terms of Thornton's<sup>27</sup> structure zone model. According to the model, as the substrate temperature is increased, small grains combine and grow into larger grains at the T zone as a consequence of increased adatom mobility. Larger grains make the surface rougher as confirmed by the SEM photograph in Fig. 6(d).

Let us consider the substrate effect. Inspection of data in Figs. 2–5 and Tables I–IV suggests that the NiCr-coated substrate yields the smoothest CoCr film surface and the weakest thickness dependence compared with other substrates under the same deposition conditions. We have analyzed the structure of NiCr and fitted the reciprocal lattice constants measured from the TEM diffraction pattern in Fig. 7(a) to those of f.c.c., b.c.c. and h.c.p. structures. We found that the best fit is obtained with h.c.p. as shown in Fig. 8. In fitting the h.c.p. structure, we have assumed that the  $c$  axis is along the film normal so that only the  $(hk0)$  planes are seen. Such a texture was also observed from TEM diffraction pattern for CoCr films<sup>14</sup>. It is interesting to compare the nearest atomic distances for cobalt, chromium, nickel

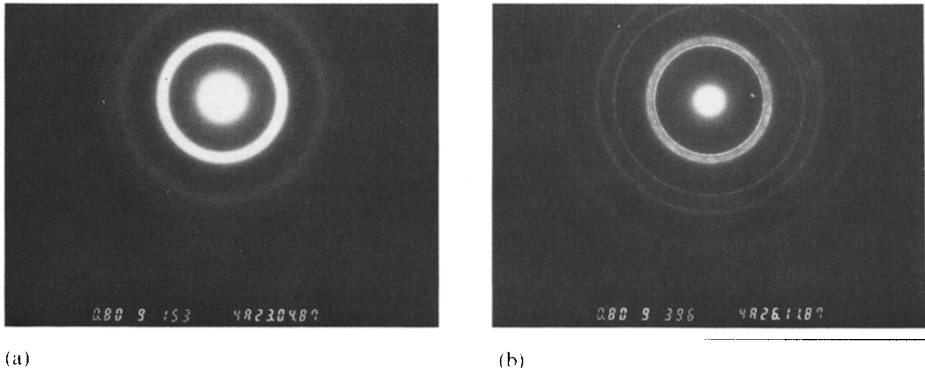


Fig. 7. (a) TEM diffraction data of NiCr deposited on carbon-coated copper grids. The beam energy is 200 kV. (b) TEM diffraction data for CoCr deposited on carbon-coated grids. The electron beam energy is 200 kV.

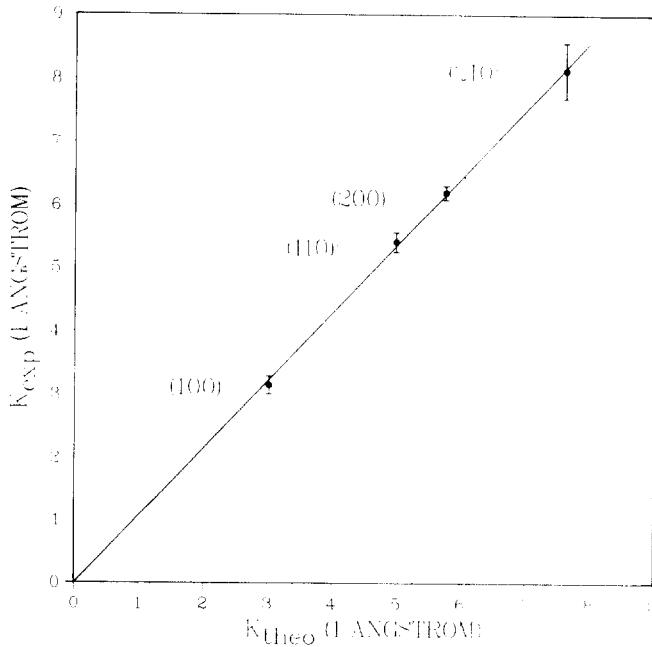


Fig. 8. Fit of the TEM diffraction data to the h.c.p. structure.  $K_{\text{theo}}$  is the reciprocal lattice constant calculated for the h.c.p. structure.  $K_{\text{exp}}$  is determined from the TEM experiment. The film is assumed to have a texture with the  $c$  axis normal to the film surface so that only the  $(hk0)$  peaks are seen.

and titanium (taken from the periodic table) with those of the alloyed films (determined from TEM data of the present study). For h.c.p. of cobalt, titanium, NiCr and CoCr the nearest atomic distance is the lattice constant of the basal plane. As can be seen from Table V, the match of the non-magnetic NiCr lattice to the CoCr lattice is better than that of titanium to CoCr. We conclude that the reduction of the initial layer effect is due to epitaxial growth of CoCr on NiCr.

TABLE V

NEAREST ATOMIC DISTANCES FOR COBALT, CHROMIUM, TITANIUM, NICKEL, CoCr (20 at.% Cr) AND NiCr (50 at.% Cr)

Material	Structure	Lattice constant (Å)
Co	H.c.p.	2.51
Cr	B.c.c.	2.49
Ni	F.c.c.	2.49
Ti	H.c.p.	2.95
CoCr	H.c.p.	2.52
NiCr	H.c.p.	2.35

The lattice constants for cobalt, chromium, nickel and titanium are from the periodic table and those for NiCr and CoCr are from TED data in Fig. 7.

## ACKNOWLEDGMENTS

We acknowledge the financial support to this work from National Science and Engineering Research Council. One of us (Z.L.) wishes to thank the University of British Columbia for financial assistance through graduate fellowships.

## REFERENCES

- 1 S. Iwasaki and Y. Nakamura, *IEEE Trans. Magn.*, 13 (1977) 1272.
- 2 R. D. Fisher, J. C. Allen and J. L. Pressesky, *IEEE Trans. Magn.*, 22 (1986) 352.
- 3 Z.-M. Li, J. F. Carolan, R. C. Thompson and R. R. Parsons, *Thin Solid Films*, 154 (1987) 431.
- 4 U. Hwang, Y. Uchiyama, K. Ishibashi and T. Suzuki, *Thin Solid Films*, 147 (1987) 231.
- 5 R. Ludwig, K. Kastner, R. Kukla and M. Mayr, *IEEE Trans. Magn.*, 23 (1987) 94.
- 6 M. Mayr, K. Kastner, R. Ludwig, R. Kukla and R. Ludwig, *IEEE Trans. Magn.*, 23 (1987) 131.
- 7 D. P. Ravipati, W. G. Haines, J. M. Sivertsen and J. H. Judy, *J. Appl. Phys.*, 61 (1987) 3149.
- 8 Y. Niimura, S. Nakagawa and M. Naoe, *IEEE Trans. Magn.*, 23 (1987) 68.
- 9 D. P. Ravipati, J. M. Sivertsen and J. H. Judy, *IEEE Trans. Magn.*, 22 (1986) 1152.
- 10 H. Hoffmann, L. Kochanowsky, H. Mändl, K. Kastner, M. Mayer, W. D. Münz and K. Röhl, *IEEE Trans. Magn.*, 21 (1985) 1432.
- 11 M. Sagoi, R. Nishikawa and T. Suzuki, *IEEE Trans. Magn.*, 22 (1986) 1335.
- 12 K. Ouchi and S. Iwasaki, *J. Appl. Phys.*, 57 (1985) 4013.
- 13 E. R. Wuori and J. H. Judy, *IEEE Trans. Magn.*, 20 (1984) 774.
- 14 Z. Li, *Ph.D. Thesis*, The University of British Columbia, 1988.
- 15 B. T. Sullivan, *Ph.D. Thesis*, The University of British Columbia, 1987.
- 16 B. T. Sullivan and R. R. Parsons, *Proc. 14th Int. Conf. on Metallurgical Coatings, San Diego, CA*, in *Thin Solid Films*, 15 (1987) 281.
- 17 B. T. Sullivan and R. R. Parsons, *J. Vac. Sci. Technol.*, A5 (1987) 3399.
- 18 D. E. Aspnes, *Am. J. Phys.*, 50 (1982) 704.
- 19 D. E. Aspnes, *Phys. Rev. B*, 33 (1986) 677.
- 20 P. N. Sen, C. Scala and M. H. Cohen, *Geophysics*, 46 (1981) 781.
- 21 T. Tanaka and H. Masuya, *Jpn. J. Appl. Phys.*, 26 (1987) 897.
- 22 D. E. Aspnes, *Proc. Soc. Photo-Opt. Instrum. Eng.*, 276 (1981) 188.
- 23 S. Honda, N. Yamashita, M. Ohkoshi and T. Kusuda, *IEEE Trans. Magn.*, 20 (1984) 791.
- 24 M. Ishizuka, T. Komoda, S. Tsuchimoto, M. Yoshikawa, S. Ishio and M. Takahashi, *J. Magn. Mater.*, 35 (1983) 286.

- 25 H. Maeda, *J. Appl. Phys.*, *54* (1983) 2429.
- 26 D. A. Glocker, W. E. Yetter and J.-S. Gau, *IEEE Trans. Magn.*, *22* (1986) 331.
- 27 J. A. Thornton, in R. F. Bunshah (ed.), *Deposition Technologies for Films and Coatings*, Noyes, 1982.